



[www.sciencemag.org/cgi/content/full/332/6029/580/DC1](http://www.sciencemag.org/cgi/content/full/332/6029/580/DC1)

Supporting Online Material for

**Surface-Generated Mesoscale Eddies Transport Deep-Sea Products  
from Hydrothermal Vents**

Diane K Adams,\* Dennis J McGillicuddy Jr., Luis Zamudio, Andreas M Thurnherr,  
Xinfeng Liang, Olivier Rouxel, Christopher R German, Lauren S Mullineaux

\*To whom correspondence should be addressed. E-mail: [dadams@whoi.edu](mailto:dadams@whoi.edu)

Published 29 April 2011, *Science* **332**, 580 (2010)  
DOI: 10.1126/science.1201066

**This PDF file includes:**

Materials and Methods

SOM Text

Figs. S1 to S6

Table S1

References

**Other Supporting Online Material for this manuscript includes the following:**  
(available at [www.sciencemag.org/cgi/content/full/332/6029/580/DC1](http://www.sciencemag.org/cgi/content/full/332/6029/580/DC1))

Movies S1 and S2

## Supporting Online Material

Materials and Methods

Supporting Text

Figs. S1, S2, S3, S4, S5, S6

Table S1

SOM References

Legends Movies S1, S2

Movies S1, S2

## Materials and Methods

**Time-series larval and geochemical fluxes.** Subsurface moorings were positioned within the axial trough within 10 m of the East Wall ( $9^{\circ} 50.54' N$ ,  $104^{\circ} 17.53' W$ ) and Choo Choo ( $9^{\circ} 49.61' N$ ,  $104^{\circ} 17.37' W$ ) vent sites (*S1*, *S2*). Each mooring was equipped with a McLane PARFLUX Mark 78H-21 time-series sediment trap at 4 meters above bottom (mab) with a  $0.5 \text{ m}^2$  opening, sampling settling particles on 7-day intervals between November 25, 2004 and April 21, 2005 (*S2*). On recovery, we maintained trap samples at approximately  $4^{\circ} C$  until the larvae were sorted and identified morphologically (*S3*) under a dissecting microscope to the lowest taxonomic level possible (e.g., species level for most gastropods). Only the supply of gastropod larvae assigned as endemic to hydrothermal vents, either due to species-level identification or identification to families endemic to vents, are presented.

We present East Wall larval fluxes in the main body and Choo Choo larval fluxes in supporting online material because corresponding geochemical analyses were only done on East Wall samples. Additionally, larval supply to Choo Choo is more variable because it is relatively isolated from other larval sources (*S1*).

The residual of every-other East Wall trap sample were split into fine size fractions ( $<300 \mu\text{m}$  or  $<1\text{mm}$ ) and coarse fractions ( $>300 \mu\text{m}$  or  $>1\text{mm}$ ) using nylon sieves. Each fraction was later filtered through 47 mm filters (Durapore<sup>TM</sup>,  $0.45\mu\text{m}$  Cat. No. HVLP04700), dried under class-100 laminar flow hood, and weighed to determine mass flux.

Filtered samples were dissolved to determine elemental composition by inductively coupled plasma mass spectrometry (ICP-MS) at the Woods Hole Oceanographic Institution. The filters were leached overnight with 10 ml of 8N distilled HNO<sub>3</sub> in 15 ml closed Teflon vials on a hot plate at 80°C. The solutions were then slowly evaporated to dryness. A second dissolution step using 0.5 ml of concentrated ultrapure HF and 3 ml of concentrated distilled HNO<sub>3</sub> was then used to obtain a total digestion of the particles. The solid residue was dissolved in 10 ml of 2% HNO<sub>3</sub> (Optima grade) and an aliquot was further diluted for multi-elemental ICP-MS analyses. Multi-elemental analysis of the digests was carried out on an ICP-MS Thermo-Electron Element 2 after appropriate dilution (typically 25- to 200-fold dilution depending the amount of digested materials). The detection limit of approximately 0.01 wt% for Fe, Al, Zn and 0.001wt% for Mn, Cu, and P was calculated from repeat analysis of blank filter digests. Indium was added to each sample as an internal standard to correct for changes of instrument sensitivity. Stock 1000 µg L<sup>-1</sup> standards (Specpure, Spex) of each element of interest were diluted in preparation for instrument calibration (ranging from 5 to 1000 ppb). A number of geo-reference standards (BHVO-1 and IFG) were also analyzed along with the samples to confirm analytical accuracy with is better than 5% for all element reported.

**Near-bottom current velocities.** Concurrent with the five months of larval and geochemical collections, each of the on-axis moorings (above) and a third mooring positioned 2 kilometers off-axis from East Wall, 9° 50.36' N, 104° 18.57' W, were equipped with Aanderaa current meters at 170 mab (on-axis) and 10 mab (off-axis). Currents were measured using Aanderaa RCM11 current meters recording every 30 min (East Wall and off-axis) or an Aanderaa RCM8 current meter recording every 10 min (Choo Choo). From May to July 2007, currents were measured using an Aanderaa RCM11 current meter at 9° 50.0' N, 104° 17.4' W, at 2430 m depth (70 mab), recording every 20 minutes. Mesoscale variations were assessed using low-pass filtered (150 h) current records to remove tidal and inertial frequencies. The high-frequency

residuals were also analyzed for weekly variability. All cross-correlations among observed, simulated and inferred current velocities were done in Matlab v.7.

**Statistical analyses.** We used permutation tests to determine whether the larval, mass and geochemical fluxes were significantly lower during and after (post) the velocity anomaly than expected by chance alone. The data were randomized 50,000 times and resampled to generate a density curve from which the likelihood of obtaining the observed post-anomaly mean was determined. We used the beginning of the anomalous northward currents, estimated to be March 03, 2005, as the *a priori* break point between pre- and post-anomaly.

**Satellite observations.** We performed daily objective analysis (OA) using satellite observations of sea level anomalies from Jason, Topex/Poseidon 2, ENVIRONMENTAL SATellite (Envisat), and GEOSAT Follow-On (GFO) produced by AVISO (S4) to detect mesoscale eddies in the region. We used a modified form of the correlation function proposed in by Siegel and colleagues (S5) in which the phase speed was set to zero ( $c_1=180$  km,  $c_2=600$  km,  $c_3=20$  d and  $c_4=0$ ). Since the satellite track coverage is dense, tracking the inferred eddies gives phase speeds similar to those in the literature. Sea level anomalies are presented as residuals after removal of the long term mean, including mean circulation and the geoid.

The months when anticyclones crossed the East Pacific Rise was tabulated based on published weekly objective analysis from 1993-2004 (S6) and daily objective analysis performed as above from 2004-2009.

**HYCOM Modelling.** HYCOM is the HYbrid vertical Coordinate Ocean Model, which is isopycnal in the open stratified ocean, terrain-following in shallow coastal regions, and z-level in mixed layer and unstratified regions. This generalized vertical coordinate approach is dynamic in space and time via the layered continuity equation that allows a smooth dynamical transition between the coordinate types. The HYCOM version used in this study is characterized by  $1/12^\circ$  horizontal grid resolution ( $\sim 7$  km at mid-latitude), 32 vertical hybrid layers, and it extends from

74°S to 90°N. It is forced with three-hourly winds and daily averaged heat fluxes from the Fleet Numerical Meteorology and Oceanography Center's Navy Operational Global Atmospheric Prediction System (NOGAPS) (S7), and it includes monthly rivers and turbidity forcing (S8). It integrates during the period January 2003 – June 2006. The model includes realistic bottom topography and coastline geometry that are based on a modified version of the 1/30° NRL DBDB2 topography (S9). The model uses the 5 meter isobath as a land-sea boundary, and does not include ocean data assimilation. Simulated current velocities were extracted from the approximate location of East Wall, 9° 50.5' N, 104° 17.5' W at 2350 m depth and near surface for the first ninety days of 2005.

## Supporting Text – Geochemical Analyses

Mass fluxes collected in sediment traps deployed near hydrothermal fields record integrated particulate fall-out from multiple sources, including lithogenic inputs from hydrothermal, volcanic, and continental sources, and biogenic inputs from hydrothermal and pelagic sources. Significant contributions of lithogenic volcanic or continental debris would result in a Hydrothermal Index (*SIO*),  $100 \times [\text{Al}] / ([\text{Al}] + [\text{Fe}] + [\text{Mn}])$ , above 40 due to their relatively high Al content. Since all Hydrothermal Index values remain below 32 (lower values indicate higher hydrothermal contribution; Table S1) throughout the time series, *all* samples have a strong hydrothermal component to their lithogenic content, as opposed to a volcanic or detrital component.

However, the hydrothermal lithogenic component, resulting from mineral particulates settling from the overlying plume supplied by high-temperature ‘black smoker’ venting, cannot account for the drop in mass flux observed at the end of the time series (Fig 1B). Mineral fall-out from the plume is high in Fe, Cu and Zn, which all remain relatively constant throughout the time series (Fig 1D, Table S1), suggesting that hydrothermal input from high-temperature venting did not change significantly. Consistent with a steady lithogenic hydrothermal input, P:Fe mass ratios (Table S1) fell below 0.10, which is expected when neutrally-buoyant plume particulates that include both Fe-oxyhydroxides (P:Fe ~ 0.10) and polymetallic sulfides (P:Fe ~ 0) dominate the flux (*SII*), only when total mass fluxes decreased late in the time series. Furthermore, the consistency of the lithogenic hydrothermal fluxes implies that they could not have exceeded the minimum mass flux ( $28 \text{ mg m}^{-2} \text{ d}^{-1}$ ) which is too small to resolve the observed decrease in mass flux. Significantly higher P fluxes ( $p = 0.041$ ; Table S1) and P:Fe ratios ( $p = 0.025$ ) observed pre-anomaly require that a different source that is P-rich and relatively Fe-poor account for the changes in total mass flux (Fig 1B).

With negligible continental and volcanogenic contributions and a small, constant hydrothermal lithogenic flux, as discussed above, the change in mass flux was likely due to variation of a biogenic input. Biological fluxes would also be consistent with the observed variation in P. While we can't rule out variation in biogenic input from pelagic production, estimates of pelagic fluxes at other vents, 5-50 mg m<sup>-2</sup> d<sup>-1</sup> (*S12-14*) always accounted for less than 25% of the corresponding near-vent total mass flux (*S12, S13*) – again, too low to resolve the change in mass flux observed here. Given the close proximity to communities with high levels of chemosynthetic production, we propose that our observations are most consistent with high biogenic flux from adjacent vent communities occurring pre-anomaly that was displaced and slow to re-establish post-anomaly.

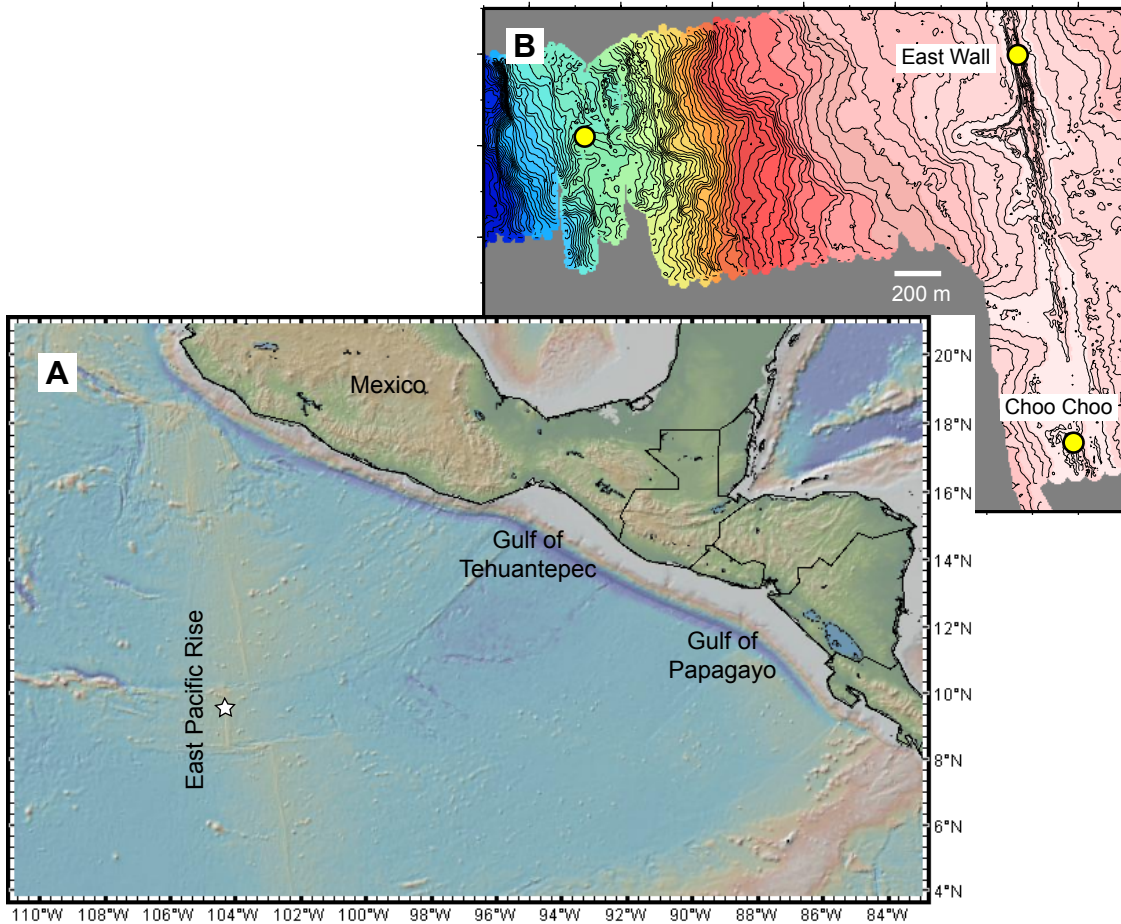


**Figure S1. Regional and ridge crest maps of the East Pacific Rise.** (A) Regional map showing the topography of Central America and the bathymetry of the East Pacific. The star marks the location of the study site, 9°N vent field. Mesoscale eddies impacting the East Pacific Rise are primarily generated in the Gulfs of Tehuantepec and Papagayo. Map created in GeoMapApp. (B) High resolution bathymetry at part of the 9°N vent field (red star in A) showing the near-vent study sites at East Wall and Choo Choo and the off-axis study site (circles). Depth contours, 2 m. Tick marks and scale bar, 200 m.

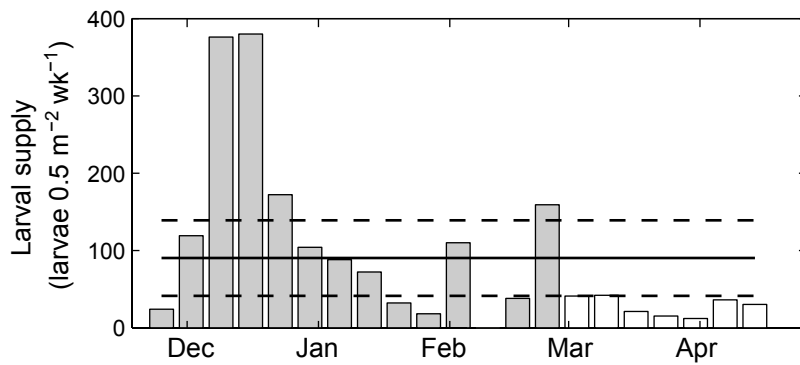


**Fig. S2 Supply of vent gastropod larvae to the Choo Choo vent site.** Solid line indicates the mean flux. Dashed lines indicate the 95% CI. Grey bars indicate samples before (pre-) the current anomaly. Open bars indicate samples during or after the current anomaly (post). Larval supply is generally more variable and lower at Choo Choo compared to East Wall because it is a relatively isolated vent site with fewer local sources (S1). Still, larval supply to Choo Choo post-anomaly was significantly lower than expected ( $p = 0.0055$ , one-sided permutation test using 50,000 randomizations).

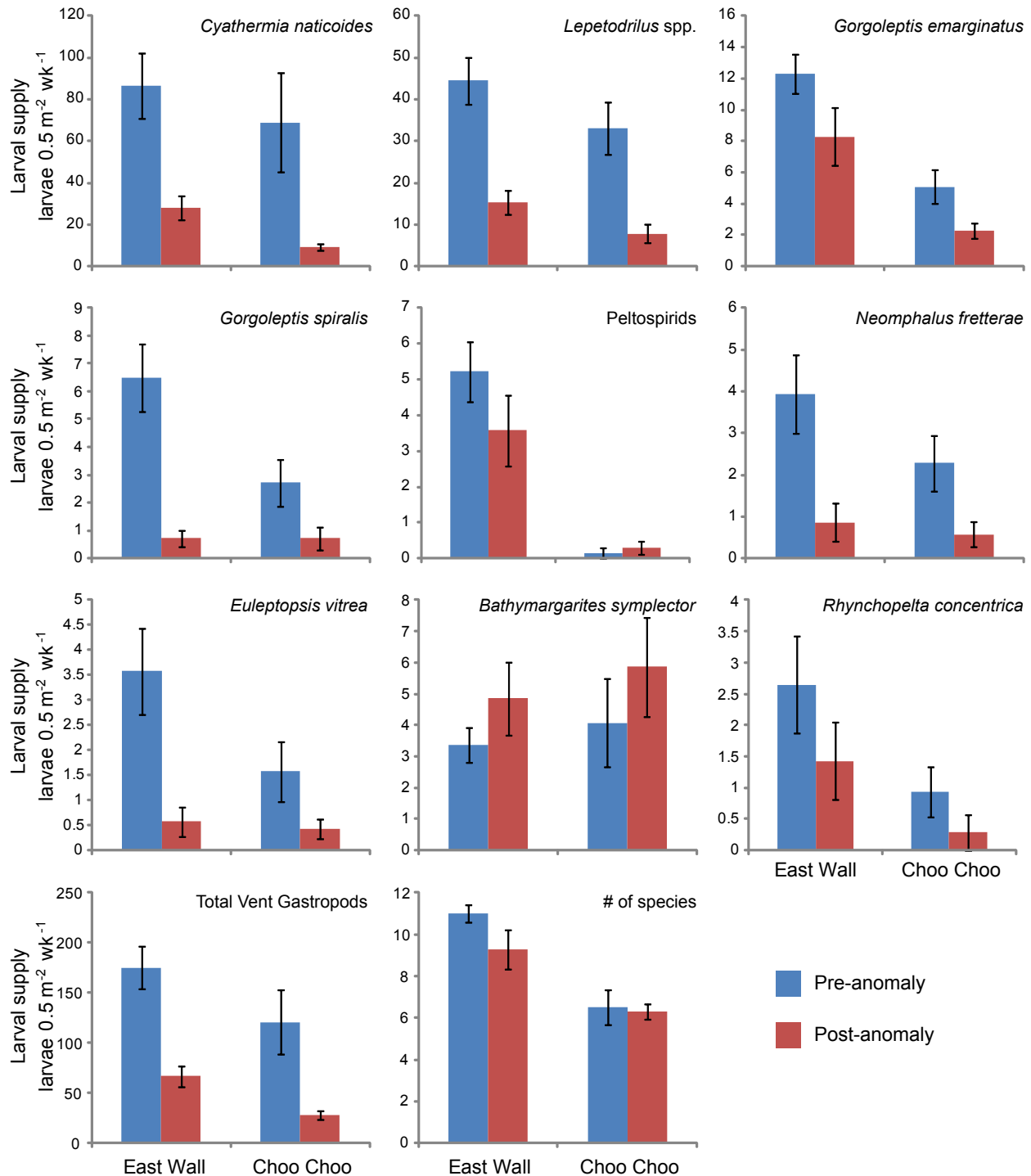


**Figure S3. Species specific supply pre- and post-anomaly.** Larval supply of selected vent gastropod species (with a mean flux greater than 2 per 0.5 m<sup>2</sup> per week), total vent gastropods, and the number of species collected before the anomaly (blue) and during and after (post) the anomaly (red) presented as the mean  $\pm$  S.E.M. The individual species typically decrease in supply post-anomaly, with the notable exception of *Bathymargarites symplector*. *B. symplector* differs from the others in its large size (320-350  $\mu$ m) (S3) and ability to feed during its larval stage. It may have enhanced swimming or behavioral capabilities relative to the other species.

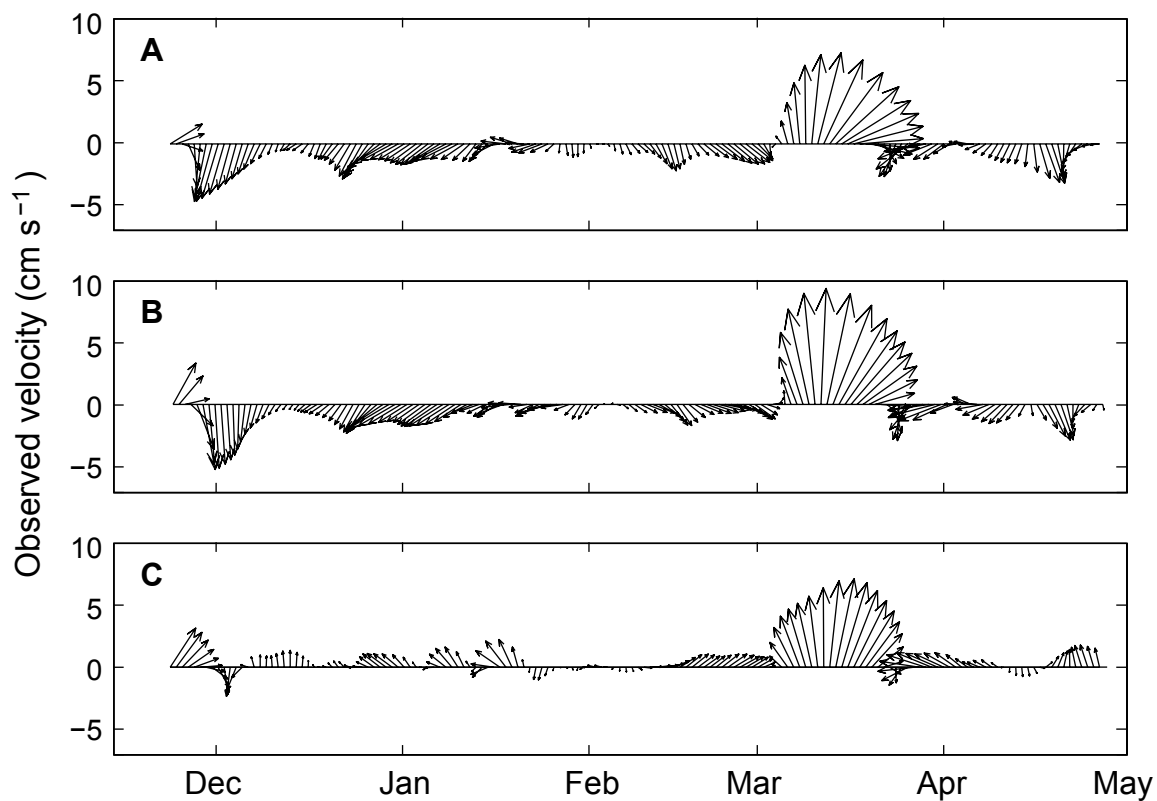


**Fig. S4** Current velocities at (A) East Wall vent site at 170 mab, (B) Choo Choo vent site at 170 mab and (C) 2 km off-axis at 10 mab all show anomalously high current speeds in March with coincident, rapid changes in direction from late February to early April.

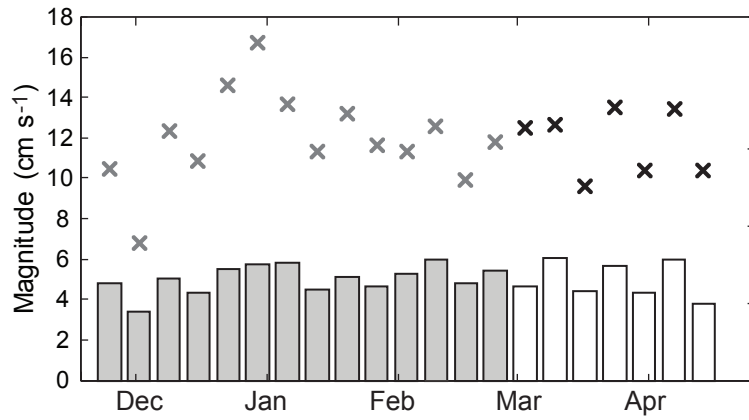


**Figure S5. High frequency motions.** Root mean square (bars) and maxima (symbols) of the residual high frequency motions in the in the 2004-2005 current meter record from East Wall, 9°N EPR. Residuals were computed by subtracting the low frequency motions (Fig. 1C) from the raw data. Grey bars and symbols indicate samples analyzed as before (pre) the current anomaly. Open bars and black symbols indicate samples during or after (post) the current anomaly. The weekly rms and maxima were not significantly lower than expected post-anomaly ( $p = 0.441$  and  $p = 0.437$ , respectively, one sided permutation test using 50,000 randomizations).

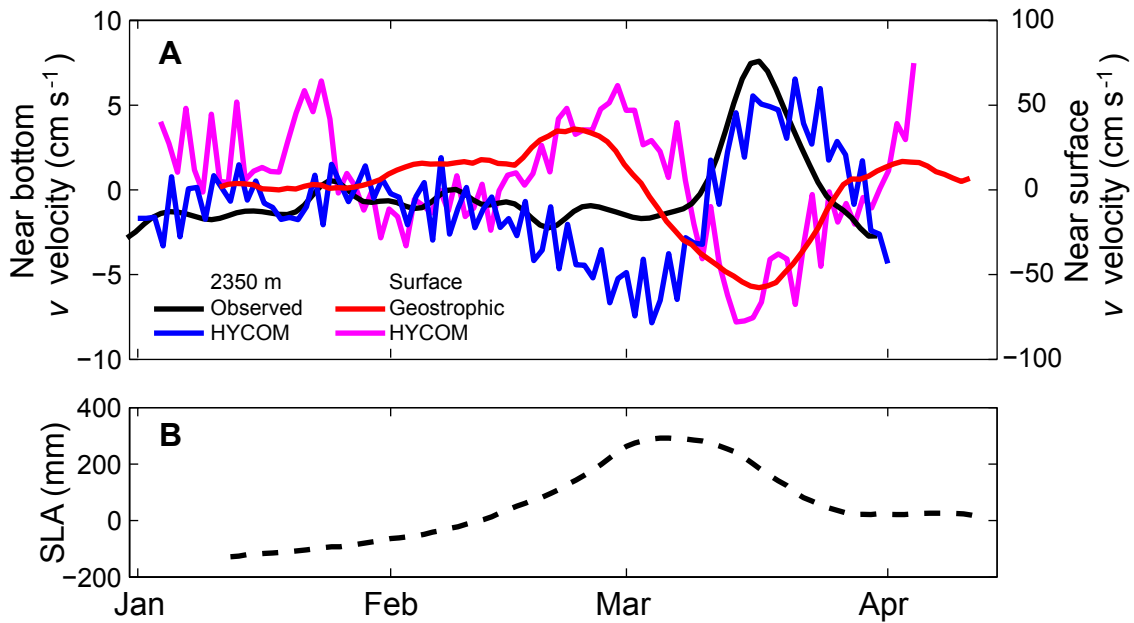


**Fig. S6** (A) Comparison of the meridional component of the observed current velocities at East Wall, 2350 m depth (black), the inferred geostrophic current velocities (red), and simulated HYCOM current velocities at 2350 m depth (blue) and near the surface (magenta) for the first 90 days of 2005. Geostrophic velocities and HYCOM surface velocities are plotted shifted 8 days and 5 days later, respectively. (B) Corresponding sea level anomaly, plotted with an 8 day shift.

**Supplementary Table 1. Geochemical fluxes at East Wall.**

Cup Number	2	4	6	8	10	12	14	16	18	20	
Start Date	2-Dec-04	16-Dec-04	30-Dec-04	13-Jan-05	27-Jan-05	10-Feb-05	24-Feb-05	10-Mar-05	24-Mar-05	7-Apr-05	
End Date	9-Dec-04	23-Dec-04	6-Jan-05	20-Jan-05	3-Feb-05	17-Feb-05	3-Mar-05	17-Mar-05	31-Mar-05	14-Apr-05	p value
Mass Flux (mg m <sup>-2</sup> d <sup>-1</sup> )	130	76	115	126	184	121	118	38	67	28	<b>0.008</b>
Fe flux (mg m <sup>-2</sup> d <sup>-1</sup> )	1.29	0.79	0.93	0.92	0.85	1.08	0.96	1.23	1.22	0.82	0.206
Al flux (mg m <sup>-2</sup> d <sup>-1</sup> )	0.66	0.39	0.46	0.47	0.40	0.46	0.46	0.28	0.56	0.34	0.143
Mn flux (mg m <sup>-2</sup> d <sup>-1</sup> )	0.15	0.11	0.11	0.13	0.10	0.15	0.14	0.10	0.21	0.08	0.440
Cu flux (mg m <sup>-2</sup> d <sup>-1</sup> )	0.048	0.025	0.020	0.023	0.018	0.020	0.016	0.031	0.013	0.009	0.217
Zn flux (mg m <sup>-2</sup> d <sup>-1</sup> )	0.035	0.019	0.031	0.050	0.021	0.031	0.030	0.035	0.022	0.030	0.441
P flux (mg m <sup>-2</sup> d <sup>-1</sup> )	0.19	0.12	0.19	0.24	0.12	0.092	0.087	0.093	0.089	0.058	<b>0.041</b>
Hydrothermal Index	32	30	31	31	29	27	29	17	28	27	<b>0.025</b>
P:Fe	0.15	0.15	0.21	0.26	0.14	0.085	0.090	0.076	0.073	0.071	<b>0.025</b>

Total mass flux and flux of six elements analyzed by ICP-MS for every other sample (cup) in the time-series sediment trap collection. The Hydrothermal Index  $\{100 \times [\text{Al}]/([\text{Al}]+[\text{Fe}]+[\text{Mn}])\}$  is a measure of the relative contribution of high-temperature hydrothermal plume fall-out, with lower numbers indicative of a higher contribution to the lithogenic component. Note that the Hydrothermal Index drastically decreases during the current anomaly (cup 16), but primarily due to a decrease in an Al-rich input rather than an increase in Fe-rich hydrothermal input. Variation in total mass flux was decoupled from the Hydrothermal Index because the Hydrothermal Index only reflects changes in the lithogenic contribution which was a small portion of the total mass flux. The p-value for fluxes that were significantly lower than expected post-anomaly compared to pre-anomaly ( $p < 0.05$ ,  $n = 10$ , permutation test with 50,000 randomizations) are in bold.

## SOM References

- S1. Adams, D. K. & Mullineaux, L. S. (2008) Supply of gastropod larvae to hydrothermal vents reflects transport from local larval sources. *Limnology and Oceanography* 53, 1945-1955.
- S2. Mullineaux, L. S., Adams, D. K., Mills, S. W. & Beaulieu, S. E. (2010) Larvae from afar colonize deep-sea hydrothermal vents after a catastrophic eruption. *Proceedings of the National Academy of Sciences of the United States of America* 107, 7829-7834.
- S3. Mills, S. W., Beaulieu, S. E. & Mullineaux, L. S. in *Woods Hole Oceanographic Institution Technical Report WHOI-2009-5* (Woods Hole Oceanographic Institution, Woods Hole, MA, 2009).
- S4. Altimeter products were produced by Ssalto/Duacs and distributed by Aviso with support from Cnes; see <http://www.aviso.oceanobs.com/>
- S5. Siegel, D., McGillicuddy, D. & Fields, E. (1999) Mesoscale eddies, satellite altimetry, and new production in the Sargasso Sea. *Journal of Geophysical Research* 104, 13359-13379.
- S6. Palacios, D. M. & Bograd, S. J. (2005) A census of Tehunatepec and Papagayo eddies in the northeastern tropical Pacific. *Geophysical Research Letters* 32, doi:10.1029/2005GL024324.
- S7. Rosmond, T. E., Teixeira, J., Peng, M., Hogan, T. F. & Pauley, R. (2002) Navy Operational Global Atmospheric Predictions System (NOGAPS): Forcing for ocean models. *Oceanography* 15, 99-108.
- S8. Kara, A. B., Wallcraft, A. J. & Hurlburt, H. E. (2005) How does solar attenuation depth affect the ocean mixed layer? Water turbidity and atmospheric forcing impacts on the simulation of seasonal mixed layer variability in the turbid Black Sea. *Journal of Climate* 18, 389-409.
- S9. [http://www7320.nrlssc.navy.mil/DBDB2\\_WWW](http://www7320.nrlssc.navy.mil/DBDB2_WWW)
- S10. Boström, K., Peterson, M. N. A., Joensuu, O. & Fisher, D. E. (1969) Aluminium-poor ferromagnesian sediments on active oceanic ridges. *Journal of Geophysical Research* 74, 3261-3270.
- S11. Feely, R. A., Trefry, J. H., Lebon, G. T. & German, C. R. (1998) P/Fe and V/Fe ratios in hydrothermal precipitates: Potential new paleo-proxies for dissolved phosphate in seawater. *Geophysical Research Letters* 25, 2253-2256.
- S12. German, C. R., Colley, S., Khripounoff, A., Klinkhammer, G. P. & Palmer, M. R. (2002) Hydrothermal sediment trap fluxes: 13°N, East Pacific Rise. *Deep Sea Research I* 49, 1921-1940.

- S13. Khripounoff, A. et al. (2008) Temporal variation of currents, particulate flux and organism supply at two deep-sea hydrothermal fields of the Azores Triple Junction. *Deep-Sea Research I* 55, 532-551.
- S14. Cowen, J. P. et al. (2001) Ascending and descending particle flux from hydrothermal plumes at Endeavour Segment, Juan de Fuca Ridge. *Deep Sea Research I* 48, 1093-1120.

## **Legends Movies S1, S2**

**Movie S1.** Daily objective analysis of sea level anomaly in the tropical East Pacific showing an initial period early in the study with little eddy activity followed by the development of predominantly anticyclonic mesoscale eddies during the winter in the Gulfs of Tehuantepec and Papagayo off the coast of Central America. Eddies propagated across the East Pacific Rise (white line) and hydrothermal vent fields (circles) including the study site (star) in mid February through the end of the time series. (mpeg; 6.7 MB; higher resolution movie deposited in Marine Geoscience Data System, <http://www.marine-geo.org/portals/ridge2000/>)

**Movie S2.** HYCOM model output showing sea surface height (SSH) anomaly and bottom currents from to 15 Jan (year day 15) to 27 March 2005 (year day 86). Note the relatively weak bottom currents at the beginning of the time series, followed by strong currents in coherent structures as large sea surface height anomalies develop in the latter half of the time series. A deep cyclonic feature developed just to the south of the anticyclone by mid-February. The propagation of this deep cyclone appeared to be impeded by the East Pacific Rise, such that the anticyclone crossed the ridge before the deep cyclone – consistent with the lag between the observed near-bottom velocity anomaly and the inferred geostrophic velocities. The bottom currents associated with the eddy field were complex and included both cyclonic and anticyclonic features and large connecting flows that persisted for weeks. (mpeg; 6 MB; higher resolution movie deposited in Marine Geoscience Data System, <http://www.marine-geo.org/portals/ridge2000/>)